CrystEngComm

PAPER

View Article Online
View Journal | View Issue

Cite this: *CrystEngComm*, 2018, **20**, 3228

Novel stable metal–organic framework photocatalyst for light-driven hydrogen production†

Qi Yu,‡ Hong Dong, ‡ Xin Zhang, ‡ Ya-Xin Zhu, Jian-Hui Wang, Feng-Ming Zhang * and Xiao-Jun Sun*

Received 12th March 2018,
Accepted 5th May 2018

DOI: 10.1039/c8ce00386f

rsc.li/crystengcomm

A novel MOF formulated as $[Dy_2(abtc)(H_2O)_2(OH)_2]\cdot 2H_2O$ (H_4abtc = 3,3′,5,5′-azobenzene tetracarboxylic acid) was successfully synthesized, in which a dye-like ligand was integrated as a photosensitizer into MOFs by the reaction with Dy^{3+} ions (dye-based Dy-MOF). The ultra-stable dye-based Dy-MOF possesses a HOMO–LUMO gap of 2.17 eV as determined by UV-vis spectrum with absorbed edge at 570 nm. The dye-based Dy-MOF shows high catalytic activity for the UV-vis light driven hydrogen production, attributed to the porous structure and light harvesting from the dye-like ligand. The band-edge positions of the crystals of the dye-based Dy-MOF were studied *via* cyclic voltammetry (CV) to further verify the principle of photocatalytic hydrogen production. Furthermore, the exceptional thermal and pH stability of the dye-based Dy-MOF makes it possible to use them as photocatalysts in water. On using Pt cocatalyst, the UV-vis light photocatalytic hydrogen evolution rate of the dye-based Dy-MOF reaches 21.53 μmol h^{-1} g^{-1}. In addition, the as-prepared dye-based Dy-MOF materials also exhibited good stability and recycling performance.

Introduction

In consideration of the energy shortage and environmental pollution, enormous efforts have been put into the exploitation of new energy resources. Among the new energy resources, hydrogen is a promising alternative to replace fossil fuels with high combustion enthalpy and environmentally friendly characteristics. The research of photocatalytic hydrogen production from water splitting has attracted considerable attention for converting the abundant solar energy into chemical fuels.[1–4] Research efforts so far have been focused on using various types of semiconductors and regulating their electronic and optical properties. Nowadays, the development of new photocatalysts for the water splitting reaction is still an extreme challenge.

Metal–organic frameworks (MOFs) are porous materials composed of metal ions or clusters and organic linkers.[5] Taking advantage of the high surface and tunable pore volumes, MOFs have been widely used in various potential applications such as gas storage,[6–8] gas separation,[9,10] drug delivery,[11–13] and proton-conductivity.[14,15] Currently, possible applications of catalysis have been focussed in the field of coordination reactions, such as H_2 production,[16,17] O_2 production,[18] CO_2 reduction[19,20] and organic conversions.[21,22] Among them, hydrogen production is a promising way to solve the energy and environmental problems. Although MOFs possess this significant property, only a few studies on MOFs have demonstrated the conversion of solar energy into chemical energy until now.

The light harvesting units called photosensitizers, which are used to capture solar photons and release photoelectrons, play major roles in photocatalysis for hydrogen production.[23,24] In an attempt to introduce photosensitizers into MOFs for efficient photocatalytic activities, two common approaches have been employed. One is to select the photosensitizers as organic ligands to construct MOFs, such as 2-aminoterephthalate and porphyrins. A porous amino-functionalized Ti(IV) metal–organic framework (Ti-MOF-NH_2)[25,26] was synthesized successfully for photocatalytic hydrogen production with triethanolamine (TEOA) as a sacrificial electron donor. Furthermore, the MOF of the same main group element, *i.e.*, Zr(IV) containing MOFs formed by 2-aminoterephthalate ligands (UIO-66-NH_2) also exhibited efficient photocatalytic activity for hydrogen generation in methanol.[27] A new water-stable porphyrin-based Al-MOF[28] performed visible-light driven hydrogen generation in the

School of Materials Science and Engineering, College of Chemical and Environmental Engineering, Harbin University of Science and Technology, Harbin 150040, PR China. E-mail: zhangfm80@163.com, sunxiaojun@hrbust.edu.cn

† Electronic supplementary information (ESI) available: FT-IR, XRD, SEM, TGA, crystal data, photocurrent response curve and characterization of after reaction available. CCDC 1425437. For ESI and crystallographic data in CIF or other electronic format see DOI: 10.1039/c8ce00386f

‡ Qi Yu, Hong Dong and Xin Zhang contribute equally to this work and should be considered co-first authors.

presence of Pt nanoparticles as co-catalyst and MV^{2+} (*N*,*N*′-dimethyl-4,4′-bipyridinium) as the electron acceptor from water. Another approach was incorporating MOFs with photosensitizers, including $Ru(tpy)_2$, $[Ru(dcbpy)(bpy)_2]Cl_2$ and $[Ir(ppy)_2(bpy)]Cl$, *via* direct synthesis methods.[29–32] When these light absorbing metal complexes were incorporated in MOFs, excellent photocatalytic hydrogen evolution activity under visible light irradiation was displayed. At present, it must be mentioned that dye-sensitized Zr-MOF[33] and Ni-MOF[24] also have been successfully synthesized *via* absorbed or directly added rhodamine B and fluorescein (F1) for photocatalytic hydrogen production under irradiation. Inspired by these studies, a dye-like ligand can be designed and integrated as a light sensitizer and a catalytic site into MOFs to generate and improve the photoactivities and simultaneously enhance their insolubility and stability. The striking feature of this strategy is that a simple system without the involvement of complex electron transfer and co-catalyst, but possessing more effective light harvesting ability.

Herein, we designed and synthesized a dye-based MOF and applied it for efficient photocatalytic hydrogen evolution. In this study, 3,3′,5,5′-azobenzene tetracarboxylic acid (H_4-abtc) was chosen as an organic linker to construct a novel 3D MOF by the reaction with Dy^{3+} ions. Moreover, the dye-based Dy-MOF also exhibited efficient photocatalytic hydrogen production with Pt as the co-catalyst. With the cocatalysts combined intimately, the electron–hole pairs activated by light would be easily dissociated and transferred into the active sites to participate in hydrogen evolution reactions (Scheme 1). The as-obtained photocatalyst exhibited remarkable H_2 production rate of 21.53 μmol h^{-1} g^{-1} in H_2O solution with an outstanding stability and cyclability.

Results and discussion

Synthesis and characterization

Dye-based Dy-MOF was achieved by the reaction of $DyCl_3{\cdot}6H_2O$ and Na_4abtc in DMF–water mixed solvent at 170 °C for three days. Excellent yields of $[Dy_2(abtc)(H_2O)_2(OH)_2]{\cdot}2H_2O$ were formed under the above reaction conditions. The symmetric and asymmetric stretching vibrations at 1398, 1606 and 1549 cm^{-1} of the carboxylate groups of the dye-based Dy-MOF are observed from the infrared spectra (Fig. S1†). Compared to that of H_4abtc, the absence of the carboxylate based characteristic peaks at around 1705 cm^{-1} in the infrared spectrum of the dye-based Dy-MOF indicates the deprotonation and consequent coordination to the metal ions.[34] In an attempt to investigate the thermal stability of the framework, thermogravimetric analysis (TGA) was carried out in N_2 atmosphere from ambient temperature to 800 °C, as shown in Fig. S2.† The result of thermal gravimetric analysis indicated that the dye-based Dy-MOF lost approximately 10% weight before 400 °C, corresponding to the loss of coordinated and free H_2O molecules. After 400 °C, the framework of Dy-MOF began to collapse. As shown in Fig. S3,† the powder X-ray diffraction patterns of the as-made samples for the dye-based Dy-MOF match well with those of the simulated diffraction patterns obtained from the single-crystal X-ray data, verifying that pure phases were obtained. The SEM image (Fig. S4†) exhibits the dye-based Dy-MOF with regular prism morphology. Furthermore, the porosity of the as-synthesized dye-based Dy-MOF was investigated by N_2 absorption experiments at 77 K (Fig. S5 and S6†). The saturation uptake for Dy-MOF is 75.21 cm^3 g^{-1}, while the Brunanuer–Emmett–Teller (BET) surface area is 237.42 m^2 g^{-1}, demonstrating its permanently porous structure.

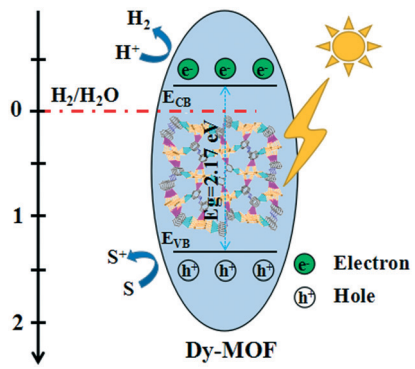

Scheme 1 The schematic illustration of photocatalytic hydrogen production reaction over the dye-based Dy-MOF under UV-vis light illumination.

Crystal structure

X-ray analysis performed on a single crystal of the dye-based Dy-MOF revealed a 3D structure crystallizing in the monoclinic system with a space group of *P*21/*n*. The asymmetric unit of the dye-based Dy-MOF contains one Dy^{3+}, half an $abtc^{4-}$ ligand, one μ_3-OH group, one coordinated water molecule and one lattice water molecule. All Dy atoms in the structure are eight-coordinated by one bidentate chelating carboxylate, two bidentate bridge carboxylate, two –OH and two H_2O molecules (Fig. 1a, b and S7†). The Dy–O bond lengths range from 2.301(8) to 2.441(4) Å, which are in agreement with the previously reported Dy–O bond length.[34,35] Two adjacent Dy atoms along the *b*-axis with red plane are bridged by two bidentate bridge carboxylate groups to form the 1D chain. The 1D chain is further extended to a 2D net-plane along the *a*-axis with the green plane chelated by one bidentate chelating carboxylate group. Then, in the vertical direction, the 2D plane is further extended to a 3D structure by the connection of the μ_3-OH groups, which bond to the metal ions from the upper layers and other metal ions from the lower layers. It is noteworthy that by inspection of the 3D framework, approximate channels occupied by H_2O molecules along the *b*-axis with dimensions of ~3.0 × 5.5 Å are exhibited in Fig. 1c.

A better insight into the nature of this novel framework can be obtained by a topological approach by reducing the framework to simple node-and-connection nets. In the structure of the dye-based Dy-MOF, Dy^{3+} ions and O atoms are

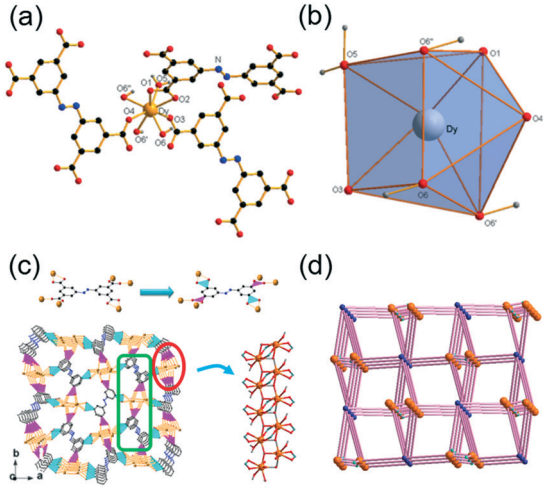

Fig. 1 (a and b) Connection mode of ligands with metal ions in the dye-based Dy-MOF. (c) The connection of 2D plane extended to 3D structure. (d) Topological analysis of the dye-based Dy-MOF.

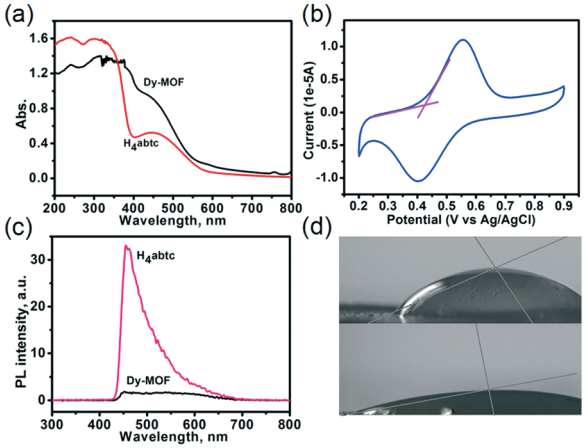

Fig. 2 (a) UV-visible spectra of the dye-based Dy-MOF and H_4abtc ligand. (b) Cyclic voltammetry curve of the dye-based Dy-MOF. (c) PL spectra of the dye-based Dy-MOF and H_4abtc ligand with excitation wavelength of 380 nm. (d) The differences in hydrophilicity between the dye-based Dy-MOF and H_4abtc ligand using contact angle measurements.

primarily present in the framework. Each Dy^{3+} ion connects to three $abtc^{4-}$ anions from ligands and three O atoms from H_2O molecules, which can be considered as 6-connected nodes. If we consider the connection of $abtc^{4-}$ anions in the structure, each $abtc^{4-}$ anion links six Dy^{3+} ions to act as a 6-connected node. The resultant structure of the dye-based Dy-MOF is a 6-nodal net with the Schläfli symbol of $(4^7{\cdot}6^6{\cdot}8^2)$ for Dy^{3+} ions (Fig. 1d), which is a novel topological structure that has never been reported.

Photocatalysis and mechanism

In the process of photocatalysis for hydrogen production, some components are typically involved. The first component is the energy gap that can separate the electrons and holes under irradiation and the energy levels that are satisfied by the redox reactions of protons. The values of the highest occupied molecular orbital (HOMO) and lowest unoccupied molecular orbital (LUMO) energy levels of the dye-based Dy-MOF are significant for their applications in photocatalytic hydrogen production. The UV-vis spectra of the dye-based Dy-MOF were recorded with well-defined optical adsorption associated with the LUMO–HOMO gap, which can be assessed at 2.17 eV based on the relation $Eg = 1240/\lambda$. As anticipated, the dye-based Dy-MOF shows a broad absorption band with the edge above 570 nm attributed to the π–π^* transition in organic ligands (Fig. 2a), indicating good light-harvest ability. Cyclic voltammetry (CV) was utilized with a carbon paste electrode in a 1 M Na_2SO_4 solution at room temperature at a scan rate of 50 mV s^{-1} to further confirm the energy levels. The redox potential at 0.43 V *vs.* Ag/AgCl can be estimated to be assigned to the HOMO energy level in Fig. 2b. As far as we know, light was absorbed by MOFs and then, the electrons and holes in the HOMO separated and the electrons could be excited into the LUMO.[36] As a result, the LUMO of the dye-based Dy-MOF is −1.74 V *vs.* Ag/AgCl as described above, which is more negative than the redox potential of H^+/H_2.[37]

Taking together the energy gap and energy level values, we can infer that the dye-based Dy-MOF has the ability of reducing protons to realize photocatalytic hydrogen production. Furthermore, the inhibiting recombination of the photoinduced electron–hole pairs of the dye-based Dy-MOF was tested by PL measurements. With the excitation wavelength of 380 nm, the PL emission peak of H_4abtc ligand showed a maximum at around 460 nm (Fig. 2c). However, the PL of the dye-based Dy-MOF was almost quenched, indicating a rapid charge transfer with the dye-based Dy-MOF, thus suppressing the radiative decay process in the excited state of the ligand.

In addition, the photocurrent response curve of the dye-based Dy-MOF was plotted *versus* Ag/AgCl under visible light irradiation. The photocurrent for all the investigated samples displayed a significant boost as soon as the light was turned on, whereas it decayed to the baseline when the light was switched off. The rapid, stable, and invertible photocurrent responses were employed in a switch-on and switch-off cycle several times (Fig. S8†). Surface hydrophilicity experiments of the dye-based Dy-MOF and H_4abtc ligand were carried out. As shown in Fig. 2d, the dye-based Dy-MOF shows smaller contact angle of 21.5° than 57.0° for the H_4abtc ligand, indicating a more hydrophilic surface of the dye-based Dy-MOF brought about by the –OH groups on the photocatalyst, which will improve water adsorption and subsequent proton reduction. Finally, the water stability of the samples was tested. Fortunately, the dye-based Dy-MOF maintained its structural characters when soaked in water solution for 48 h with pH = 3–14, adjusted using concentrated H_2SO_4 and NaOH. The exceptional stability of the dye-based Dy-MOF makes it possible to produce hydrogen in water (Fig. 3).

The photocatalytic activity of the dye-based Dy-MOF materials and H_4abtc ligand were evaluated by photocatalytic hydrogen evolution under UV-vis light irradiation. Fig. 4a shows the hydrogen production yields under the irradiation

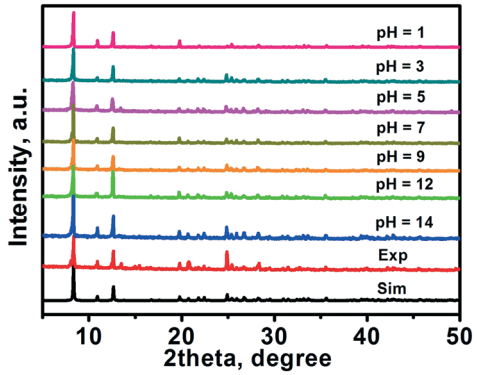

Fig. 3 The pH stability of the dye-based Dy-MOF.

of UV-vis light for 5 h. Clearly, the dye-based Dy-MOF (0.8% Pt) material exhibited excellent hydrogen production activity, which surpassed those of the dye-based Dy-MOF (0 Pt) and H_4abtc ligand. Furthermore, we also studied the influence of co-catalyst loading in photocatalytic activity. The results showed that the loading of 0.8% Pt resulted in the highest photocatalytic activity (Fig. S9†). In the photocatalytic evaluation system (Fig. S10†), the gas circulation system was at room temperature, and the temperature of the cooling circulating water was controlled at 5 °C. As shown in Fig. 4a, the dye-based Dy-MOF exhibited high activity with the hydrogen production rate of 107.65 μmol g^{-1} in 5 h (21.53 μmol g^{-1} h^{-1}), which is superior to that of most of the reported MOF-based catalysts without dye-like ligands reported previously, such as UiO-66 and ZIF-8,[38,39] but lower than that of some porphyrin-based MOFs. Moreover, it should be noted that Dy-MOF crystals used for photocatalytic hydrogen production in this study may exhibit lower hydrogen production ability than nanoscale materials. Notably, due to the excellent pH stability, the dye-based Dy-MOF exhibited more stable performance in the cycling measurements of H_2 generation than that of most reported MOF-based catalyst materials.[40,41] As shown in Fig. 4b, in the case of the H_2 recycling test, it was observed that up to the 3rd cycle, the activity was almost constant. Furthermore, the sample was characterized by XRD and FT-IR analyses after the reaction (Fig. S11–S13†). Compared with the fresh catalyst, no distinct change was observed by these characterization methods, demonstrating the durable property of the dye-based Dy-MOF photocatalyst.

Conclusions

In summary, a novel dye-based Dy-MOF with extra stability for different pH solutions was successfully synthesized. Benefiting from the appropriate energy level of the framework and the excellent light harvesting ability from the dye-like ligand, the dye-based Dy-MOF with the assistance of Pt co-catalyst exhibits prominent photocatalytic activity for hydrogen production under UV-vis irradiation. The PL results also demonstrated the rapid charge transfer and low recombination rate of photocurrent carriers in the dye-based Dy-MOF. Photocurrent responses were rapid, stable, and invertible in the dye-based Dy-MOF. In addition, the as-prepared dye-based Dy-MOF materials exhibited good stability and recycling performance. This study not only highlights the intrinsic role of MOFs in the enhanced photocatalytic performance for H_2 production, but also provides significant guidance to take full advantage of predominant properties of the MOFs in designing more efficient photocatalysts.

Experimental

Materials and chemicals

All the chemicals were purchased and used without further purification. 3,3′,5,5′-Azobenzene tetracarboxylic acid (H_4abtc) was synthesized according to the method reported in the literature. Na_4abtc was synthesized as follows: H_4abtc (3.58 g) was dissolved in 40 mL H_2O and then, NaOH (1.60 g) was gradually added. The mixture was stirred until pH = 7 was obtained. The resultant orange solution was recovered by filtration. To this solution, EtOH was added until large amounts of yellow solids appeared. The products were recovered by filtration, washed with EtOH and dried at room temperature.

Synthesis of $[Dy_2(abtc)(H_2O)_2(OH)_2]\cdot 2H_2O$

The dye-based Dy-MOF was synthesized by a solvothermal method. A mixture of $Dy(NO_3)_3\cdot 6H_2O$ (0.033 mmol, 15.0 mg), Na_4abtc (0.025 mmol, 11.0 mg), DMF (4 mL), and H_2O (11

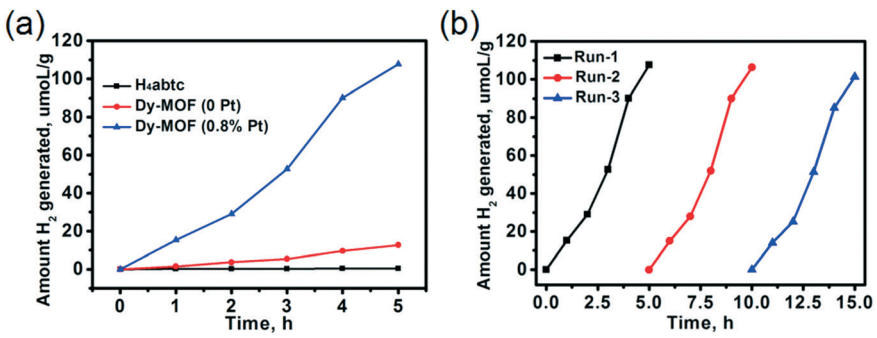

Fig. 4 (a) Photocatalytic H_2 generation rates for the dye-based Dy-MOF (0 and 0.8 wt% Pt) and H_4abtc ligand. (b) The cycling runs of the dye-based Dy-MOF catalyst under visible light irradiation for 15 h.

mL) was magnetically stirred for 40 min. Then, the resultant mixture was sealed in a 25 mL Teflon-lined stainless steel autoclave for 72 h at 443 K under autogenous pressure. Then, the reaction mixture was slowly cooled to room temperature at a rate of 5 °C per hour to obtain orange block crystals (yield: 70.63%).

Photocatalytic reactions

The photocatalytic experiments were carried out in a 200 mL Pyrex reactor *via* a photocatalytic H_2 production activity evaluation system (CEL-SPH2N, CEAUlight, China). In the photocatalytic reactions, the photocatalyst (50 mg) was dispersed in 100 mL of 30 vol% triethanolamine (TEOA) aqueous solution. Then, 3% Pt nanoparticles were deposited on the dye-based Dy-MOF as cocatalysts, which were rooted in H_2PtCl_6 by a photodeposition method. Before irradiation, the system was vacuumed for at least 30 min using a vacuum pump to completely remove the dissolved oxygen. Then, the resultant mixtures were irradiated for 5 h with a 300 W Xe lamp ($\lambda >$ 320 nm) and stirred at room temperature. After the reaction, the evolved gas was analyzed by an on-line gas chromatograph of SP7800 with a TCD detector. Cooling water was used to maintain the temperature at 5 °C.

Conflicts of interest

There are no conflicts to declare.

Acknowledgements

This study was financially supported by the National Natural Science Foundation of China (No. 21501036 and 21676066).

Notes and references

1 P. Luan, M. Xie, X. Fu, Y. Qu, X. Sun and L. Jing, *Phys. Chem. Chem. Phys.*, 2015, **17**, 5043–5050.
2 Y. Qu, W. Zhou, Y. Xie, L. Jiang, J. Wang, G. Tian, Z. Ren, C. Tian and H. Fu, *Chem. Commun.*, 2013, **49**, 8510–8512.
3 A. Kudo and Y. Miseki, *Chem. Soc. Rev.*, 2009, **38**, 253–278.
4 D. Y. Shi, R. Zheng, M. J. Sun, X. R. Cao, C. X. Sun, C. J. Cui, C. S. Liu, J. W. Zhao and M. Du, *Angew. Chem., Int. Ed.*, 2017, **56**, 14637–14641.
5 D. Tian, Q. Chen, Y. Li, Y.-H. Zhang, Z. Chang and X.-H. Bu, *Angew. Chem., Int. Ed.*, 2014, **53**, 837–841.
6 D. Alezi, Y. Belmabkhout, M. Suyetin, P. M. Bhatt, L. J. Weselinski, V. Solovyeva, K. Adil, I. Spanopoulos, P. N. Trikalitis, A. H. Emwas and M. Eddaoudi, *J. Am. Chem. Soc.*, 2015, **137**, 13308–13318.
7 H.-L. Jiang and Q. Xu, *Chem. Commun.*, 2011, **47**, 3351–3370.
8 S. Liu, L. Sun, F. Xu, J. Zhang, C. Jiao, F. Li, Z. Li, S. Wang, Z. Wang, X. Jiang, H. Zhou, L. Yang and C. Schick, *Energy Environ. Sci.*, 2013, **6**, 818–823.
9 H. Kim, J. Park and Y. Jung, *Phys. Chem. Chem. Phys.*, 2013, **15**, 19644–19650.
10 J. Liu, P. K. Thallapally, B. P. McGrail, D. R. Brown and J. Liu, *Chem. Soc. Rev.*, 2012, **41**, 2308–2322.
11 P. Horcajada, C. Serre, G. Maurin, N. A. Ramsahye, F. Balas, M. Vallet-Regí, M. Sebban, F. Taulelle and G. Férey, *J. Am. Chem. Soc.*, 2008, **130**, 6774–6780.
12 F.-M. Zhang, H. Dong, X. Zhang, X.-J. Sun, M. Liu, D.-D. Yang, X. Liu and J.-Z. Wei, *ACS Appl. Mater. Interfaces*, 2017, **9**, 27332–27337.
13 R. Ananthoji, J. F. Eubank, F. Nouar, H. Mouttaki, M. Eddaoudi and J. P. Harmon, *J. Mater. Chem.*, 2011, **21**, 9587–9594.
14 Y. Ye, W. Guo, L. Wang, Z. Li, Z. Song, J. Chen, Z. Zhang, S. Xiang and B. Chen, *J. Am. Chem. Soc.*, 2017, **139**, 15604–15607.
15 F. M. Zhang, L. Z. Dong, J. S. Qin, W. Guan, J. Liu, S. L. Li, M. Lu, Y. Q. Lan, Z. M. Su and H. C. Zhou, *J. Am. Chem. Soc.*, 2017, **139**, 6183–6189.
16 W. C. Chen, C. Qin, X. L. Wang, Y. G. Li, H. Y. Zang, Y. Q. Jiao, P. Huang, K. Z. Shao, Z. M. Su and E. B. Wang, *Chem. Commun.*, 2014, **50**, 13265–13267.
17 T. Wang, Q. Zhou, X. Wang, J. Zheng and X. Li, *J. Mater. Chem. A*, 2015, **3**, 16435–16439.
18 R. E. Hansen and S. Das, *Energy Environ. Sci.*, 2014, **7**, 317–322.
19 H. Fei, M. D. Sampson, Y. Lee, C. P. Kubiak and S. M. Cohen, *Inorg. Chem.*, 2015, **54**, 6821–6828.
20 X. Kang, Q. Zhu, X. Sun, J. Hu, J. Zhang, Z. Liu and B. Han, *Chem. Sci.*, 2016, **7**, 266–273.
21 A. Dhakshinamoorthy, A. M. Asiri and H. Garcia, *Chem. Soc. Rev.*, 2015, **44**, 1922–1947.
22 A. Dhakshinamoorthy, M. Alvaro and H. Garcia, *Catal. Sci. Technol.*, 2011, **1**, 856–867.
23 Q. Zhang, D. Chen, X. He, S. Huang, J. Huang, X. Zhou, Z. Yang, J. Li, H. Li and F. Nie, *CrystEngComm*, 2014, **16**, 10485–10491.
24 Y. Feng, C. Chen, Z. Liu, B. Fei, P. Lin, Q. Li, S. Sun and S. Du, *J. Mater. Chem. A*, 2015, **3**, 7163–7169.
25 Y. Horiuchi, T. Toyao, M. Saito, K. Mochizuki, M. Iwata, H. Higashimura, M. Anpo and M. Matsuoka, *J. Phys. Chem. C*, 2012, **116**, 20848–20853.
26 T. Toyao, M. Saito, Y. Horiuchi, K. Mochizuki, M. Iwata, H. Higashimura and M. Matsuoka, *Catal. Sci. Technol.*, 2013, **3**, 2092.
27 C. Gomes Silva, I. Luz, F. X. Llabres i Xamena, A. Corma and H. Garcia, *Chem. – Eur. J.*, 2010, **16**, 11133–11138.
28 A. Fateeva, P. A. Chater, C. P. Ireland, A. A. Tahir, Y. Z. Khimyak, P. V. Wiper, J. R. Darwent and M. J. Rosseinsky, *Angew. Chem., Int. Ed.*, 2012, **51**, 7440–7444.
29 C.-C. Hou, T.-T. Li, S. Cao, Y. Chen and W.-F. Fu, *J. Mater. Chem. A*, 2015, **3**, 10386–10394.
30 P. Buckley, *Yearbook of Psychiatry and Applied Mental Health*, 2009, vol. 2009, pp. 344–345.
31 T. Toyao, M. Saito, S. Dohshi, K. Mochizuki, M. Iwata,

H. Higashimura, Y. Horiuchi and M. Matsuoka, *Chem. Commun.*, 2014, **50**, 6779–6781.
32 C. Wang, K. E. deKrafft and W. Lin, *J. Am. Chem. Soc.*, 2012, **134**, 7211–7214.
33 J. He, J. Wang, Y. Chen, J. Zhang, D. Duan, Y. Wang and Z. Yan, *Chem. Commun.*, 2014, **50**, 7063–7066.
34 F. Zhang, P. Yan, X. Zou, J. Zhang, G. Hou and G. Li, *Cryst. Growth Des.*, 2014, **14**, 2014–2021.
35 M. Fang, L. Chang, X. Liu, B. Zhao, Y. Zuo and Z. Chen, *Cryst. Growth Des.*, 2009, **9**, 4006–4016.
36 M. A. Nasalevich, M. van der Veen, F. Kapteijn and J. Gascon, *CrystEngComm*, 2014, **16**, 4919.
37 Y. C. Li, H. Z. Zhong, R. Li, Y. Zhou, C. H. Yang and Y. F. Li, *Adv. Funct. Mater.*, 2006, **16**, 1705–1716.
38 C. G. Silva, I. Luz, F. X. L. I. Xamena, A. Corma and H. Garcia, *Chem. – Eur. J.*, 2010, **16**, 11133–11138.
39 L. He, L. Li, T. T. Wang, H. Gao, G. Z. Li, X. T. Wu, Z. M. Su and C. G. Wang, *Dalton Trans.*, 2014, **43**, 16981–16985.
40 M. C. Wen, K. Mori, T. Kamegawa and H. Yamashita, *Chem Commun.*, 2014, **50**, 11645–11648.
41 Y. Horiuchi, T. Toyao, M. Saito, K. Mochizuki, M. Iwata, H. Higashimura, M. Anpo and M. Matsuoka, *J. Phys. Chem. C*, 2012, **116**, 20848–20853.